Journal of Sound and Vibration 327 (2009) 333–353

Contents lists available at ScienceDirect

Journal of Sound and Vibration

journal homepage: www.elsevier.com/locate/jsvi

Improvement of lightweight floating ceiling design with optimum stiffener and isolator locations

C.K. Hui *, C.F. Ng

Department of Civil and Structural Engineering, Hong Kong Polytechnic University, Hung Hom, Kowloon, Hong Kong

ARTICLE INFO

Article history:
Received 26 February 2009
Received in revised form
17 July 2009
Accepted 20 July 2009
Handling Editor: C.L. Morfey
Available online 15 August 2009

ABSTRACT

In this paper, a new design concept of a lightweight floating ceiling with a special arrangement of stiffener beams and isolators is proposed to enhance vibration isolation performance. The key design parameters of resonant frequency of bending and mode shape factor on vibration transmission are determined with some simple formulae. Structural vibrations and noise radiation are evaluated with finite element models (FEM) for various designs. The optimum ceiling designs are applied in a studio, and field measurements with reliable frequency range of 30–400 Hz are conducted to confirm the theoretical results.

The analyses ascertain that four design features ensure the optimum vibration isolation performance: the stiffener beams must be installed at the nodal line of fundamental bending resonance of the plate; smaller panels should be applied instead of a large panel covering the whole area of the ceiling, and joints should be free; the isolators should be placed at the nodal point of the bending mode of the plate; and the fundamental bending resonance frequency must not match the modal critical frequency. The proposed stiffened wooden panel design achieved a noise and vibration reduction of 20 dB in the frequency range of 40–100 Hz, and was better than the performance of a concrete floating floor.

1. Introduction

Stiffened lightweight floating systems are widely applied in ships, trains, buses, airplanes, and houses to reduce the transmission of structure-borne noise to the receivers.

The vibration isolation performance of lightweight panels, however, is still unsatisfactory in the low frequency range [1]. Blazier and Dupree [2] point out that there is an increasing acceptance of wooden construction in many countries, and thus low frequency noise is still a critical issue.

The results from Hveem [3] and Sipari [4] demonstrate that: (1) lightweight floating floor systems have no improvement on impact sound insulation below 160 Hz; (2) floating ceilings have limitations on sound insulation due to the bending resonance frequency at around 30 Hz; (3) structural resonance frequencies of the floor system should not coincide with the acoustic resonance frequencies (30–80 Hz) in the room; (4) footfall noise is dominated by frequencies below 50 Hz. Fig. 1 summarizes the noise problem of wooden and concrete floors and the current performances of floating systems. Low frequency vibration isolation performance is also significant for train vibration isolation [5]. The vibration spectrum radiated by rail traffic is dominated by a low frequency range below 200 Hz with the peaks coming at around 40–80 Hz [6].

* Corresponding author. Tel.: +852 2766 6013; fax: +852 2334 6389.
E-mail address: catherine@hkdatacenter.com (C.K. Hui).

0022-460X/$ - see front matter © 2009 Elsevier Ltd. All rights reserved.
doi:10.1016/j.jsv.2009.07.019

Nomenclature

a	length of panel, along x-axis (m)
b	length of panel, along y-axis (m)
c	speed of sound (ms^{-1})
c_o	damping coefficient of isolator ($N(m\,s^{-1})^{-1}$)
c_r	modal damping coefficient of the rth mode ($N(m\,s^{-1})^{-1}$)
E_s	Young's modulus of stiffener beam ($N\,m^{-2}$)
E_p	Young's modulus of panel ($N\,m^{-2}$)
f	excitation frequency (Hz)
f_r	natural frequency of the rth mode (Hz)
f_{cr}	modal critical frequency of the rth mode (Hz)
F_b	excitation force on base structure (N)
h_{xm}	stiffener beam installed orthogonal to x-axis in position m ($m = 0,1..4$) (m)
h_{yn}	stiffener beam installed orthogonal to y-axis in position n ($n = 0,1..4$) (m)
i	imaginary number $\sqrt{-1}$
I_s	moment of inertia of stiffener beam (m^4)
I_p	moment of inertia of panel (m^4)
k_r	modal stiffness of the rth mode ($N\,m^{-1}$)
l_{xr}	length between the nodal points along x-axis for the rth mode (m)
l_{yr}	length between the nodal points along y-axis for the rth mode (m)
m_b	mass of base structure (kg)
m'_s	mass per unit length of stiffener beam ($kg\,m^{-1}$)
m'_p	mass per unit length of panel ($kg\,m^{-1}$)
m_r	modal mass of the rth mode (kg)
m_p	mass of panel (kg)
Q	amplitude of displacement (m)
Q_r	modal displacement of the rth mode (m)
R_r	mode shape factor of the rth mode
R_{rs}	mode shape factor of the rth mode with stiffener beam installed in y-direction
S	total area of vibrating structure (m^2)
t_f	flange thickness of rectangular hollow section of stiffener beam (m)
t_w	web thickness of rectangular hollow section of stiffener beam (m)
t_2	outside width of rectangular hollow section of stiffener beam (m)
t_3	outside depth of rectangular hollow section of stiffener beam (m)
T	vibration transmissibility
V_p	velocity of floating panel ($m\,s^{-1}$)
V_b	velocity of base structure ($m\,s^{-1}$)
$\langle \bar{V}^2 \rangle$	quadratic velocity of the vibrating structure average over the surface $(m\,s^{-1})^2$
W	sound power (W)
Z_p	impedance of floating panel ($N(m\,s^{-1})^{-1}$)
Z_o	impedance of isolator ($N(m\,s^{-1})^{-1}$)

Greek letters

ζ_r	damping ratio of the rth mode
λ	frequency parameter
ξ, η	coordinates for a point on the plate (m)
ρ	mass density of air (kg/m^3)
σ	radiation efficiency

Subscripts

b	abbreviation for the word "base"
m	$m = 0$ represents the distance of stiffener beam from edge is 0 m; $m = 1$ represents the distance of stiffener beam from edge is 0.16 m; $m = 2$ represents the distance of stiffener beam from edge is 0.32 m; $m = 3$ represents the distance of stiffener beam from edge is 0.48 m; $m = 4$ represents the distance of stiffener beam from edge is 0.64 m.
n	$n = 0$ represents the distance of stiffener beam from edge is 0 m; $n = 1$ represents the distance of stiffener beam from edge is 0.08 m; $n = 2$ represents the distance of stiffener beam from edge is 0.16 m; $n = 3$ represents the distance of stiffener beam from edge is 0.24 m; $n = 4$ represents the distance of stiffener beam from edge is 0.32 m.
o	represent for the word "isolator"
p	abbreviation for the word "panel"
rth	$r = 0$ represents vertical rigid body mode; $r = 1$ represents first symmetric bending mode in x-direction; $r = 2$ represents first symmetric mode in y-direction; $r = 3$ represents first symmetric bending mode in both x- and y-directions
s	abbreviation for the word "stiffener"

To tackle the vibration degradation effect of bending resonance, stiffener beams on floating panels have been previously investigated. Jeon and Yoo [7] found out that fibreglass reinforced plastic beams attached beneath a ceiling structure could decrease the heavyweight impact noise and vibration. Stiffener beams, however, may increase sound radiation from the panel [8,9]. Berry and Nicolas [10] confirm that the installation of stiffener beams on panels can attenuate the radiated sound power effectively, except at the first bending mode of the stiffener beam, and that the radiated sound power is not reduced due to the higher radiation efficiency at that frequency.

The present study [11], a new theoretical floating floor design achieved a vibration reduction of 20–30 dB in the frequency range of 120–600 Hz, with nodal point support for a small floating panel. This paper describes a practical floating panel design with a larger size of 0.8 m × 1.6 m, and stiffened panel was used instead of a large panel covering the whole ceiling area.

The vibration transmission and sound radiation efficiency for some design cases are studied with simple formulae. The simplified equations are used for designing floating panels in the initial stage. The effects of stiffener installation patterns

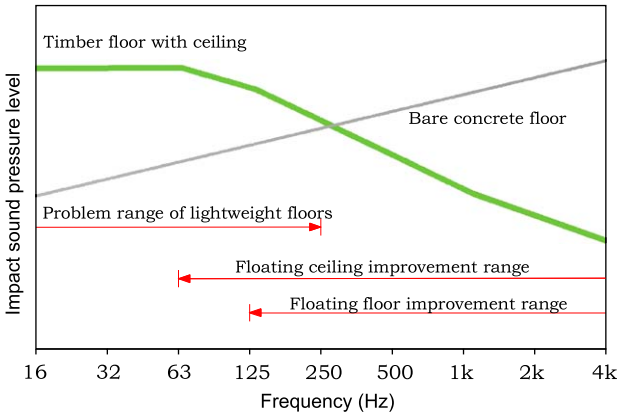

Fig. 1. The frequency range of improvements for floating floor and floating ceiling [4].

Table 1
Vibration mode shape of free–free beam structure.

Boundary conditions of beam	Mode shape equation	
Free–free	$\Psi_1(x)=\cosh\frac{\lambda_1 x}{a}+\cos\frac{\lambda_1 x}{a}-\sigma_1\left(\sinh\frac{\lambda_1 x}{a}+\sin\frac{\lambda_1 x}{a}\right)$	$\lambda_1=4.7300474$
	$\Psi_2(x)=\cosh\frac{\lambda_1 y}{b}+\cos\frac{\lambda_1 y}{b}-\sigma_1\left(\sinh\frac{\lambda_1 y}{b}+\sin\frac{\lambda_1 y}{b}\right)$	$\sigma_1=0.9825022$

Remarks: x_1 = point of excitation; x_2 = point of response, x_s = point of stiffener beam.
Mode shape factor of 1st symmetric bending mode in x-direction: $R_1=\Psi_1(x_1)\Psi_1(x_2)$.
Mode shape factor of 1st symmetric bending mode in y-direction: $R_2=\Psi_2(y_1)\Psi_2(y_2)$.
Mode shape factor of 1st symmetric bending mode in x-direction with stiffener beam installed in y-direction: $R_{1s}=\Psi_1^2(x_s)$.

on structural natural frequencies are studied with a finite element model, and the results are compared with the simple formulae in order to draw some useful guidelines for floating ceiling design.

2. Formulae for design of isolation system

2.1. Formulae of motion transmissibility

The equation for vibration transmissibility for the effects of bending resonance has been obtained from Eq. (1) in Beranek's study [12]. It is applied to the case of an isolated lightweight panel placed on a heavy base structure. Compared with the lightweight panel, the base structure is assumed to be infinitely stiff. The panel vibrates like a free–free beam for the first bending mode (Table 1).

$$\text{Vibration transmissibility } (T)=\frac{V_P}{V_b}=\left|\frac{Z_P}{Z_o}+1\right|^{-1} \tag{1}$$

where

$$Z_o=\frac{k_o}{\mathrm{i}(2\pi f)}+c_o,\quad Z_P=\left(\frac{1}{m_p\mathrm{i}(2\pi f)}+\sum_{r=1}^{N}\frac{R_r}{\frac{k_r}{\mathrm{i}(2\pi f)}+m_r\mathrm{i}(2\pi f)+c_r}\right)^{-1},\quad V_b=\frac{F_b}{m_b(2\pi f)}$$

At the first symmetric bending resonance of panel:

$$T(f_1)=B_1\frac{R_1}{\zeta_1\gamma_1^2} \tag{2a}$$

$$V_p=B_1\frac{R_1}{\zeta_1\gamma_1^2}\frac{F_b}{(2\pi f)m_b} \tag{2b}$$

where mode shape factor R_r can be estimated from Table 1, $\gamma_1 = f_1/f_o$, f_1 is first bending resonance frequency in x-direction and f_o is the vertical rigid body resonance frequency (isolator resonance); ζ_1 is the damping ratio of f_1; and $B_1 = m_1/m_p$ is dependent on the modal mass.

For Eq. (2a), the amplitude of the first symmetric bending resonance can be reduced by decreasing the mode shape factor and increasing the frequency of bending resonance. The bending resonance frequency may be increased by installing stiffener with optimum position. The significance of bending resonances on vibration isolation is also confirmed by [13].

2.2. Influence of stiffener on radiated sound

If the fundamental symmetric bending resonance frequency in x-direction is below the modal critical frequency (f_{c1}), according to [14] the radiation efficiency σ can be approximated as Eq. (3b):

$$f_{\mathrm{cr}} = \sqrt{\left(\frac{c}{2l_{xr}}\right)^2 + \left(\frac{c}{2l_{yr}}\right)^2} \tag{3a}$$

$$\sigma = \frac{0.66a^3b}{\pi^5 c^4}(2\pi f_1)^4 \tag{3b}$$

The structural radiated sound power (W) can now be obtained by using Eqs. (2) and (3b),

$$W = \rho c \langle \overline{V} \rangle^2 S\sigma = D\left(\frac{R_1 f_o}{f_1}\right)^2 \frac{a^3 b}{2} \tag{4}$$

where the quadratic velocity $\langle \overline{V} \rangle^2$ is defined by the square velocity average over vibrating structure:

$$\langle \overline{V} \rangle^2 = \frac{\int_0^b \int_0^a V_P^2 \,\mathrm{d}x\,\mathrm{d}y}{ab} \quad \text{and} \quad D = \frac{2.64B_1^2 f_0^2 \rho F_b^2 S}{\pi^3 \zeta_1^2 c^3 m_b^2}$$

The structural radiated sound power at the fundamental bending resonance frequency depends on the mode shape factor R_1 and the frequency of bending resonance f_1. Therefore, the techniques of increasing the bending resonance frequency with stiffener structure and nodal point support of the isolator can reduce the vibration magnitude as well as reduce the structural radiated sound power. It is important that radiation efficiency grows to maximum when the structural bending resonance frequency is equal to or larger than modal critical frequency. The noise radiated from the vibrating structural becomes efficient. Below the bending resonance frequency f_1, radiation efficiency for the rigid body mode is given by

$$\sigma = \frac{2\pi}{c^2} f^2 ab \tag{5a}$$

and

$$W = 1.87c^2 D \frac{R_1^2 ab f_o^2}{f^4} \tag{5b}$$

It can be seen that the radiated sound power due to rigid body mode decreases with frequency.

2.3. Approximate formulae for fundamental bending natural frequency of stiffened plate

When two stiffener beams are placed parallel to the panel in one direction symmetrically, and the mode shape of a stiffened rectangular plate is approximated by single beams along two directions, then approximate closed form solutions for natural frequencies of the first symmetric bending mode can be calculated using Eqs. (6a) for the stiffener beam installed along x-direction, and (6b) for the stiffener beam installed along y-direction. These formulae are simplified under three conditions: (1) stiffener beams are installed in a single direction; (2) the bending stiffness of stiffener beams should be at least eight times that of the panel; (3) Young's modulus of stiffener should be equal or higher than Young's modulus of panel. The equations are simplified and thus they are only applied for evaluating the trend of the natural frequency of varied stiffened panels:

$$f_1 = \frac{\lambda^2}{2\pi a^2}\left(\frac{E_s I_s}{m_p' + m_s'}\right)^{1/2} \quad \text{(For stiffener beam in } x\text{-direction)} \tag{6a}$$

$$f_1 = \frac{\lambda^2}{2\pi b^2}\left(\frac{E_p I_p}{m_p' + m_s' R_{1s}}\right)^{1/2} \quad \text{(For stiffener beam in } y\text{-direction)} \tag{6b}$$

The value of frequency parameter (λ) can be obtained from Table 1 and is detailed in [15]. On the basis of Eq. (6a), the natural frequency of bending in x-direction with the stiffener beam in the same direction (refer to Fig. 2) is determined by

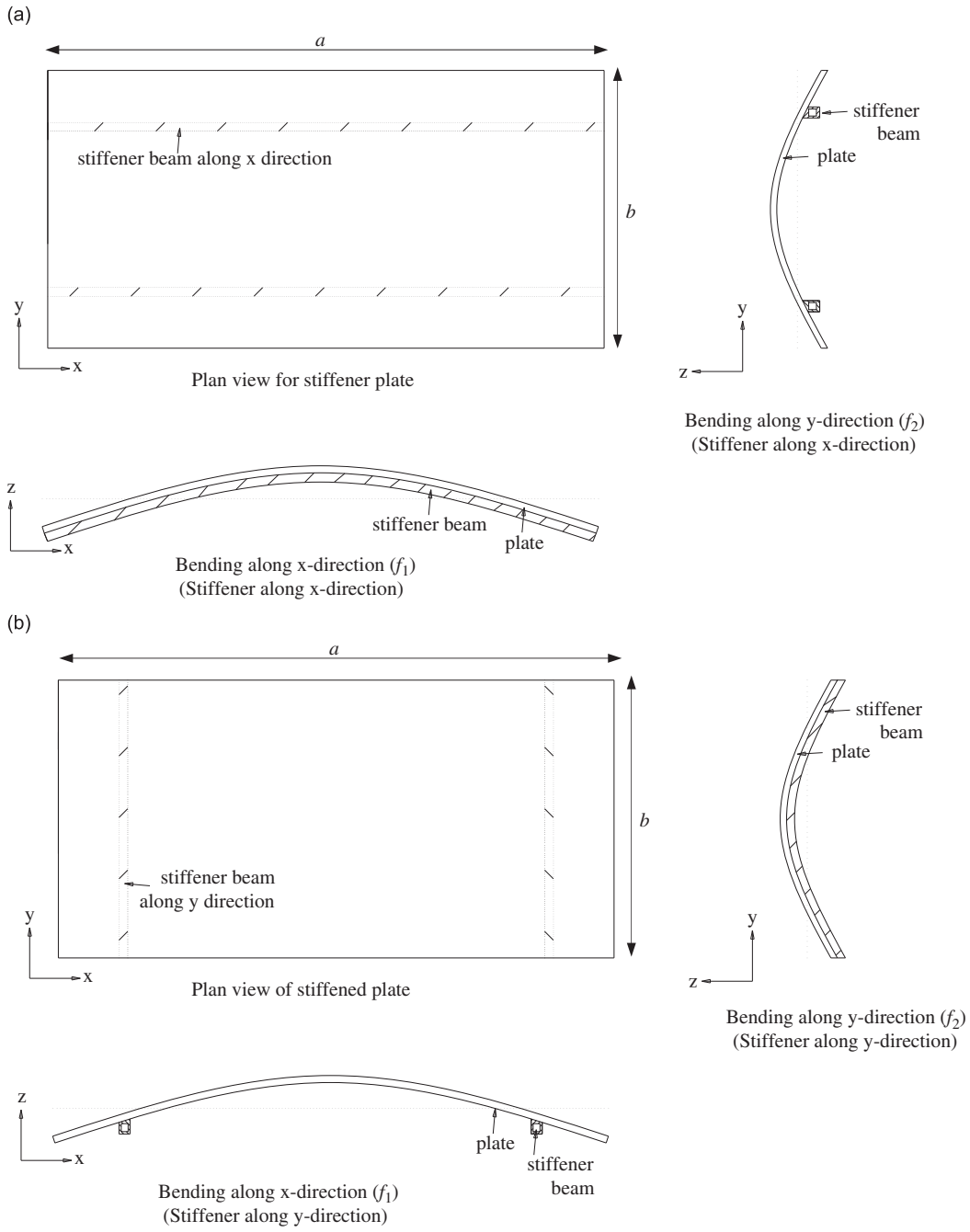

Fig. 2. The first symmetric bending mode of plate with stiffener beam installed (a) along *x*-direction (b) along *y*-direction.

the material properties of the stiffener, including Young's modulus (E_s) and their moment of inertia (I_s). The increase of mass of the plate will actually reduce the resonance frequency. Similarly, Eq. (6b) shows that the natural frequency of bending is in *x*-direction, but the stiffener beam in the opposite direction is determined by the material properties of plate E_p and I_p. The mass of stiffener is actually decreasing the resonance frequency, and thus the fundamental natural frequency of bending in *y*-direction (f_2) may become lower than that bending in *x*-direction (f_1).

3. Theoretical analysis

The effects of stiffener installation patterns on vibration behaviours are investigated with FEM (Sap2000) in order to produce some guidelines on the design of stiffener patterns for higher fundamental bending resonance frequency.

Table 2
Dimensions and material properties of floating panel design.

Material	Size (m)	Young's modulus (E) ($\mathrm{N\,m^{-2}}$)	Density (ρ) ($\mathrm{kg\,m^{-3}}$)	Possion's ratio	Loss factor
Wooden panel	length = 1.6; width = 0.8; height = 0.05	10.0×10^{9}	9.0×10^{2}	0.25	0.03
Steel stiffener	Hollow section—outside depth (t_3) = 0.05; outside width (t_2) = 0.05; flange thickness (t_f) = 3.0×10^{-3}; web thickness (t_w) = 3.0×10^{-3}	210×10^{9}	7.6×10^{2}	0.30	0.001
Wooden stiffener	Rectangular section—width = 0.05; height = 0.12	10.0×10^{9}	5.0×10^{2}	0.25	0.03

Thin shell elements and frame elements were used for the modelling of panel and stiffener beam, respectively. There are four nodes for each element and six degrees of freedom at each node: For the rectangular floating ceiling study 10 (in 1.6 m length) × 10 elements (in 0.8 m length) were applied. The elasticity of isolators was selected to give the natural frequency of 12 Hz; four isolators were placed at four corners of the plate. The boundary conditions are assumed to be free along the circumference of the plate.

The dynamic analysis of mode shapes and natural frequencies was obtained. The first symmetric bending mode in panel x-direction and first symmetric bending mode in panel y-direction should be important for vibration isolation performance.

3.1. Fundamental natural frequency of bending mode

In order to illustrate the influence of stiffener installation pattern on natural frequency of bending, a typical wooden plate with size of 1.6 m length, 0.80 m width and 0.05 m thick, and hollow section steel stiffener beam with outside depth (t_3) and outside width (t_2) of 0.05 m, flange thickness (t_f) and web thickness (t_w) of 3.0×10^{-3} m, are employed in the analysis, the input parameters for material properties are listed in Table 2. It should be noted that wooden stiffener has much higher loss factor than that of steel stiffener. It is difficult to increase damping to steel stiffener because of its high bending stiffness.

The natural frequencies and mode shapes in contour plot of the first two symmetric bending modes of the wooden floating panel without stiffened are presented in Figs. 3a and b. The first symmetric bending mode at 68.7 Hz is similar to a free–free beam in x-direction. The first symmetric bending mode at 253.8 Hz is similar to a free–free beam in y-direction. The nodal lines are marked in dotted circles in the contour plot graphs and are located at 0.22 of the length from the edge.

Ten combinations of stiffener beam installation methods are studied in this study. The methods of installation can be simply divided into two types; they are illustrated in the drawing of Figs. 4a and 5a. Type 1 includes five cases: two stiffeners, parallel to x-direction moving from the edge of the plate towards the centre, the distances "hy" are listed in Fig. 4a. Type 2 contains five cases: two stiffeners installed parallel in y-direction, and the distances "hx" are shown in Fig. 5a.

The natural frequencies of the first two symmetric bending modes of stiffened plate for the studied cases, Type 1 reinforced beam in x-direction and Type 2 reinforced beam in y-direction are shown in Figs. 4b and 5b, respectively. For Type 1, it is noted that the stiffener beams in x-direction have slight effect on the natural frequency of first symmetric bending along stiffened direction (f_1) varies from 210.1 to 227.3 Hz This phenomenon shows that the bending stiffness of floating panel in x-direction is dominated by stiffener beam.

There is an optimum location of stiffener beams obtaining higher natural frequency of bending (f_2), as shown in Fig. 4b, $h_{y2} = 0.16$ m. The reason for different natural frequencies of the first symmetric bending mode should be due to the stiffener beam in x-direction contributes additional mass to the first symmetric bending movement in y-direction (f_2). The smallest modal mass for the bending mode should be located at h_{y2}, the displacement of the mass contributed from stiffener beam is minimized due to the stiffener location as illustrated in Fig. 4b. The stiffener location is corresponded to the nodal lines presented in Fig. 3b. Comparing with the wooden panel without stiffened; the installation of stiffener beam on $h_y = 0.16$ m can achieve the highest fundamental natural frequency of bending increment from 68.7 Hz (without stiffener beam) to 227.3 Hz.

A similar trend of natural frequency of bending x- and y-directions can also be observed in Type 2 stiffener installation method. The highest fundamental natural frequency of bending can be achieved by optimum stiffener location along y-direction ($h_{x2} = 0.32$ m), which corresponds to the nodal line marked in Fig. 3a. The natural frequency of bending increases from 68.7 Hz (without stiffener beam) to 72.1 Hz; however, this frequency is still low compared with the optimum stiffener installation of Type 1 ($h_{y2} = 0.16$ m).

The lowest natural frequency of bending can be observed in the case of the stiffener beam placing at the edge since the largest modal mass and the moment of initial increase the mass effect contributed from stiffener beam.

3.2. Motion transmissibility

The highest fundamental bending resonance frequency can be achieved by the installation of a stiffener beam on a nodal line along x-direction (refer to Fig. 3b). The effects of steel stiffener and wooden stiffener (listed in Table 2) on the vibration transmissibility of wooden panels are studied. The panels are those used in Section 3.1.

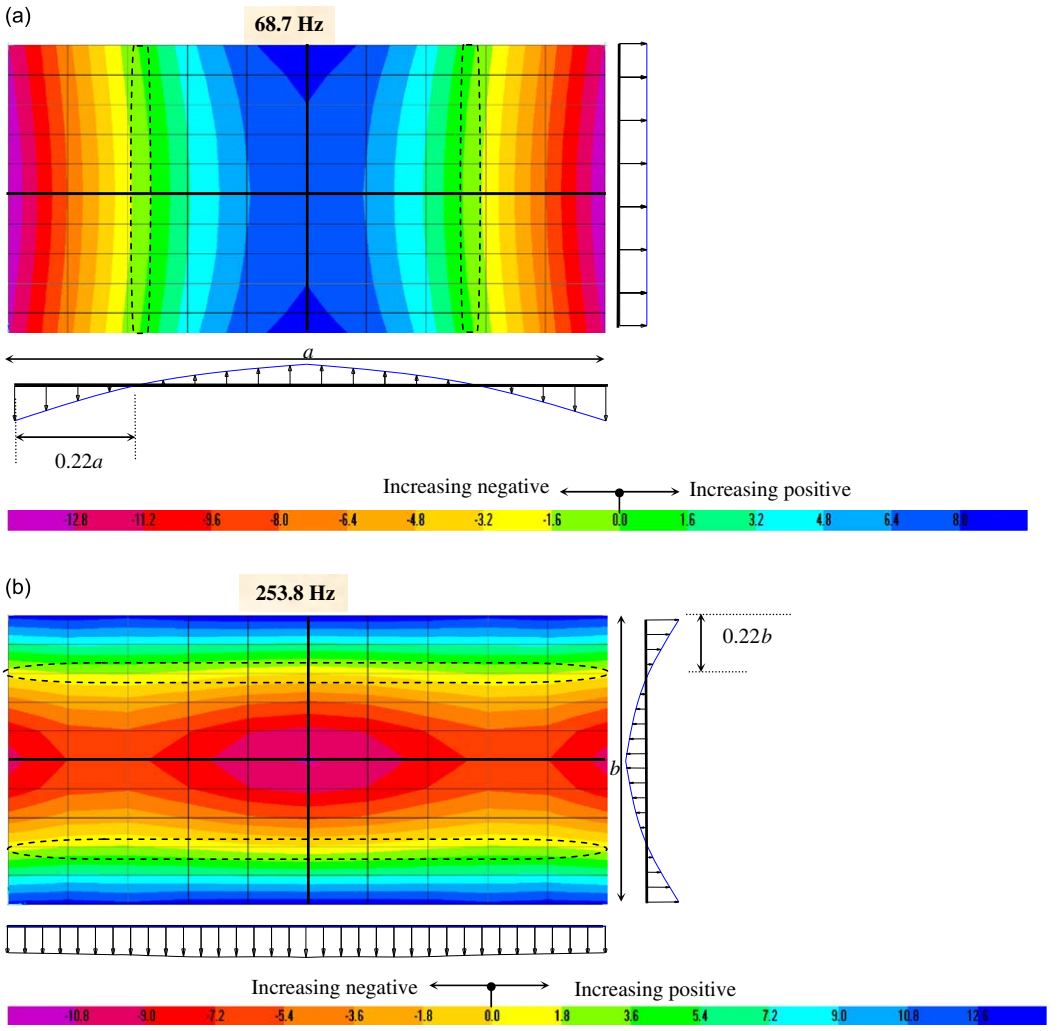

Fig. 3. Contour plot and lateral profiles for first symmetric bending mode (a) in x-direction of floating plate at 68.7 Hz, (b) in y-direction of floating plate at 253.8 Hz. The contour plot with "- - - -" notation signifying nodal lines of bending.

The motion transmissibility at centre point of the panels predicted by FEM for the three cases is shown in Fig. 6. The rigid body vibration resonances are maintained at 12 Hz for the three cases (including the panel without stiffener). For the floating wooden panel without stiffener, the peaks at 68.7 and 253.8 Hz corresponded to the natural frequency of first symmetric bending in x-direction (f_1) and y-direction (f_2), respectively. There is vibration amplification at around 69 Hz; this can be attenuated significantly by installing the stiffener beams in x-direction and along the nodal line of bending mode. The two resonance frequencies increased to 102.7 and 257.1 Hz after the installation of a wooden stiffener, and 227.3 and 257.7 Hz after the installation of a steel stiffener. There was no vibration amplification due to bending resonances.

The lowest mode shape factor can be achieved by placing isolators at nodal points of the first symmetric bending resonances in x- and y-directions (refer to Fig. 7). The motion transmissibility at centre point of the panels, and isolator placed at nodal points are presented in Fig. 8. It is obvious that the magnitude of transmissibility is attenuated significantly at two bending resonant frequencies. However, the resonance peaks are not totally eliminated because the size of isolators is larger than the area of the nodal point. The two cases of stiffened panel can achieve a good vibration reduction of around 20 dB from 40 to 100 Hz.

3.3. *Radiation efficiency*

In general, vibrating structures of wall, floors, and windows are modelled as rectangular plates simply supported in an infinite baffle. In this paper, the floating ceiling is modelled as a plate with free boundary. There are, however, very few analysis results available in the previous studies. The analytical model of radiated sound from free–free plate is developed in Appendix A [16,17]. The analysis is based on mode shapes with simple cosine function.

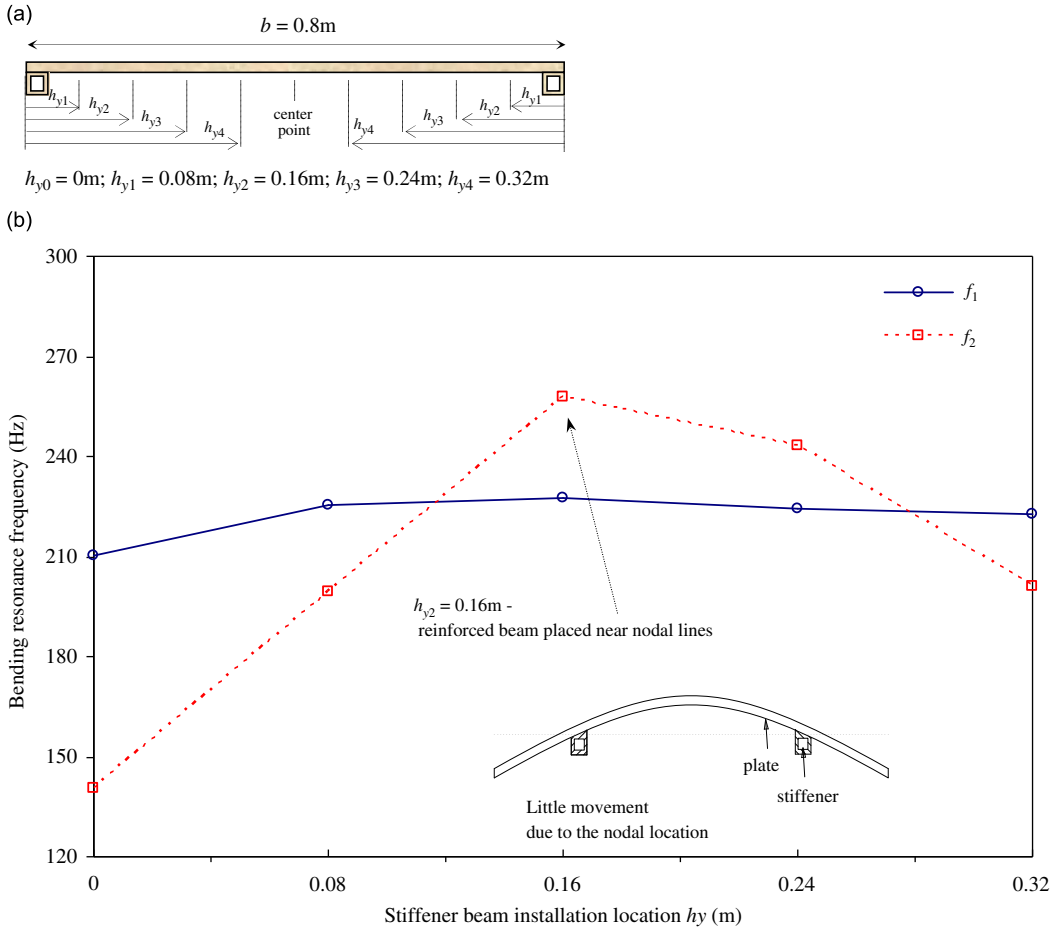

Fig. 4. (a) Stiffener installation pattern of Type 1. (b) The natural frequencies of first symmetric bending modes of wooden plate for stiffener beam installed along *x*-direction.

3.3.1. *Influence of mode shapes on radiation efficiency*

A detailed analysis of radiation efficiency in terms of major vibration mode shapes is studied and presented in Eq. (7). (The general expression is given in Eq. (A.2).)

$$Q(\xi,\eta) = Q_0 + Q_1 \cos\left(\frac{2\pi\xi}{a}\right) + Q_2 \cos\left(\frac{2\pi\eta}{b}\right) + Q_3 \cos\left(\frac{2\pi\xi}{a}\right)\cos\left(\frac{2\pi\eta}{b}\right) \tag{7}$$

The plate geometry is given in Fig. 9. The modal displacements can be found from the results of FEM. The radiation efficiency estimated from Eq. (A.8) according to modal displacements in Eq. (7) is plotted in Figs. 10–13. The radiation efficiency for the various modes of free–free plate calculated with Eq. (7) is plotted in dot–dot lines (Fig. 10), depending on the mode shapes and frequency only. Detailed studies on the radiation efficiency of a bending wave on finite plates with various boundary conditions are given by [14,18–20]. Theoretical radiation efficiency of first bending mode of the free–free panel is compared with theoretical formulae according to Ref. [14] and plotted in Fig. 10. The results are very close. It should be noted that the first bending mode of the free–free plate has lower radiation efficiency than that of the simply supported plate [14]. This low radiation efficiency results from the cancellation effects between adjacent poles of radiation in the vibration mode shapes. Furthermore, the first bending resonance frequency of the free–free plate is higher than that of the simply supported plate.

The results of radiation efficiency of the three floating panels design according to the vibration resonances are presented in Figs. 11–13 with solid lines. Those solid lines show a detailed expression of radiation efficiency that varies with frequency. These figures demonstrate the influence of changing resonance modes on radiation efficiency. There are various dips resulting from changing of resonance modes. Compared with a plain wooden panel (Fig. 11), a wooden stiffener (Fig. 12) can decrease the structural radiation efficiency. The installation of a steel stiffener (Fig. 13), however, can increase the radiation efficiency. High sound power will be generated by steel stiffened panel at around 200–315 Hz bands because the radiation efficiency is high in the region of fundamental bending resonance frequency (f_1 and f_{c1} also located at 250 Hz band).

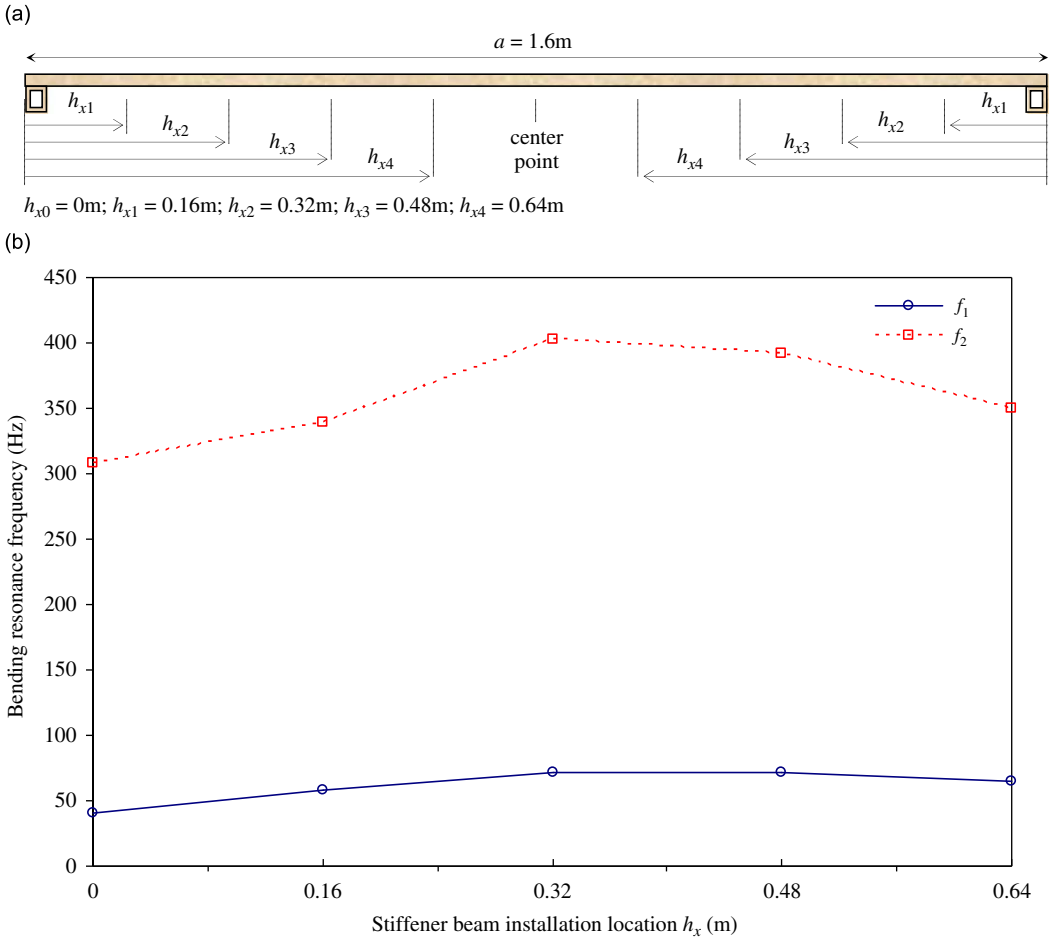

Fig. 5. (a) Stiffener installation pattern of Type 2. (b) The natural frequencies of first symmetric bending modes of wooden plate for stiffener beam installed along *y*-direction.

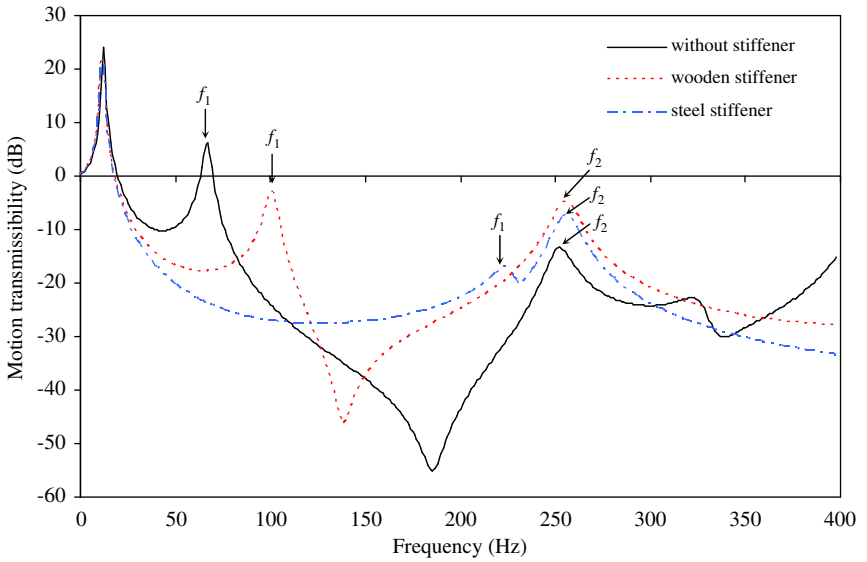

Fig. 6. Theoretical motion transmissibility of wooden panel, and stiffened wooden panel, with isolators placed at four corners (all stiffener located at $h_{y2} = 0.16$ m).

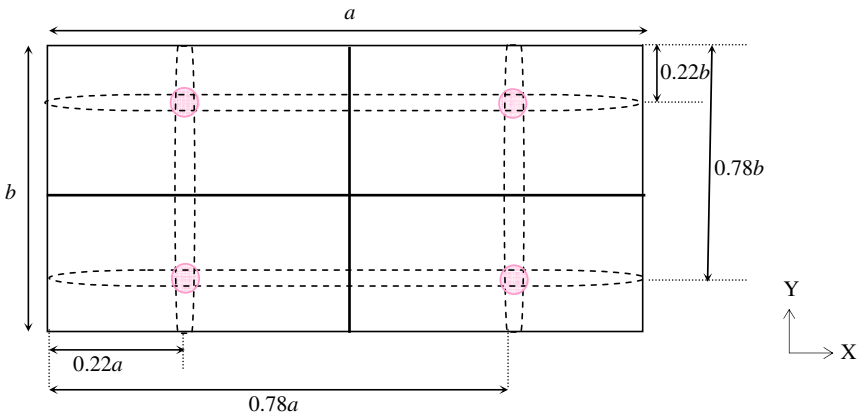

Fig. 7. The nodal points of the first symmetric bending resonances in *x*- and *y*-directions.

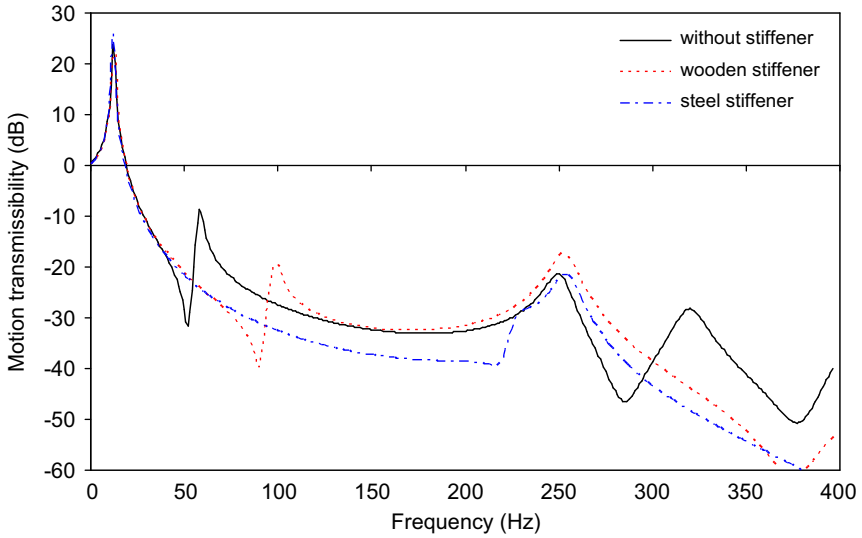

Fig. 8. Theoretical motion transmissibility of wooden panel, and stiffened wooden panel, with isolators placed at four nodal points (all stiffener located at $h_{y2} = 0.16$ m).

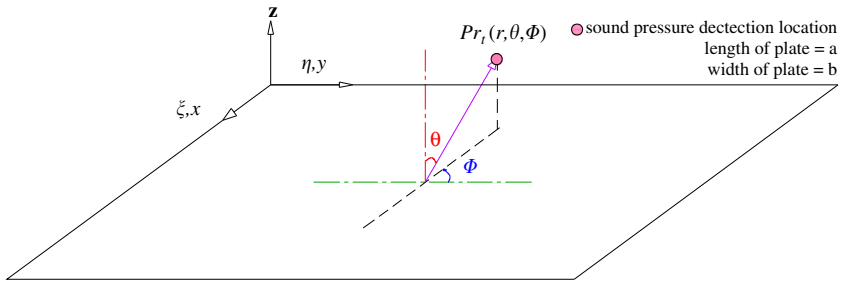

Fig. 9. Geometry on radiating side of plate.

3.4. Structural radiated sound

The practical and optimum floating ceiling design will be installed in a studio room with a volume of 3.2 m length × 3.2 m width × 4 m height as shown in Fig. 14. The base walls and floors are isolated from one another. A concrete floating floor has been used, and absorption materials are installed on the walls. The radiated sound pressure levels of the designed floating ceilings can be predicted with Eq. (A.9). The room directivity and room constant are calculated to be 2 and

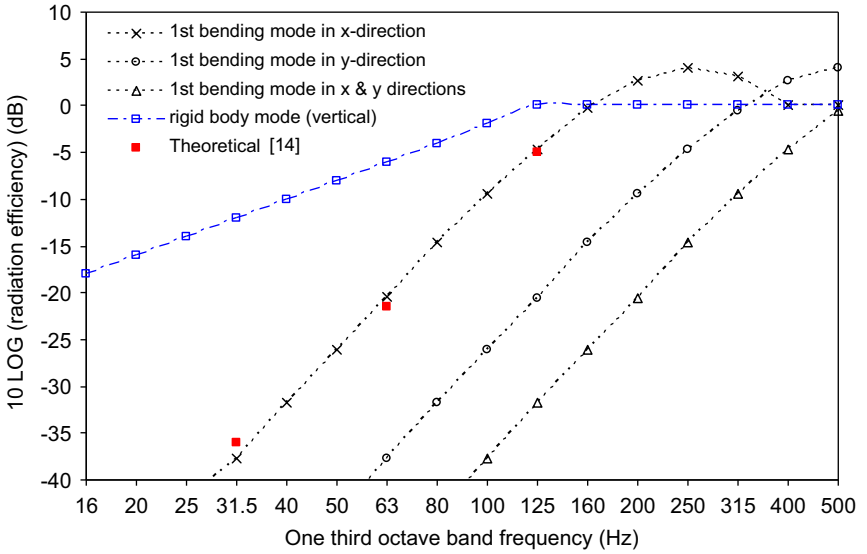

Fig. 10. Theoretical radiation efficiency for various modes of free–free plate and comparison with Ref. [14].

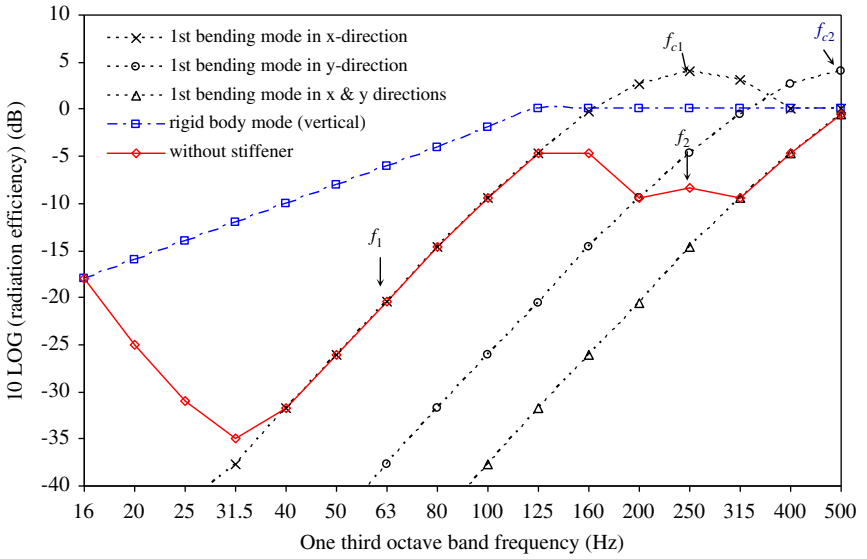

Fig. 11. Theoretical radiation efficiency of wooden panel without stiffener.

60, respectively. The input vibration magnitude is obtained by predicting the vibration on the top of the base concrete floor with the operation of the 120-N shaker.

The predicted sound pressure levels of the floating ceiling designs of the isolator placed at corner points and nodal points are presented in Figs. 15 and 16, respectively. In the graph of the corner point support panel, there are higher radiated sound pressure levels in the low frequency range below 80 Hz, especially at 63 Hz band of fundamental bending resonance frequency of the panel without stiffener. Comparing structural radiated sound pressure levels between the stiffened panel and the panel without stiffener, there is a higher radiated sound at about 250 Hz band from the steel stiffened panel. Furthermore, there is a higher radiated sound at around 100 and 125 Hz bands for the wooden stiffened panel, but the noise level is much lower than that of the panel without stiffener at 63 Hz.

As presented in Fig. 15, both the wooden stiffened panel and the non-stiffened panel have lower radiated sound at the bending resonance frequencies than the steel stiffened panel. As Table 3 reveals the main reason for this phenomenon is that the acoustic wavelength matches the structural wavelength for the steel stiffened panel; thus the bending resonance of the steel stiffened panel at 250 Hz band becomes a strong sound radiator, whereas this does not occur for the wooden stiffened panel and non-stiffened panel.

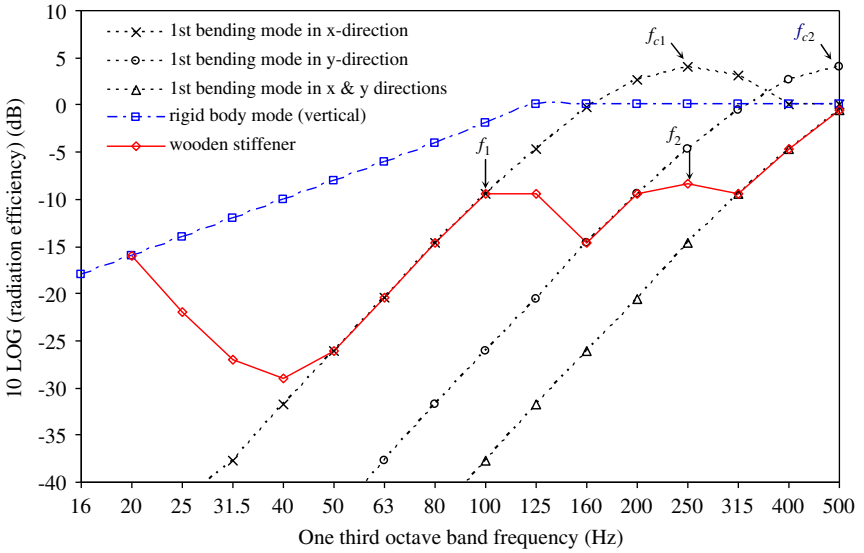

Fig. 12. Theoretical radiation efficiency of wooden panel with wooden stiffener (stiffener located at $h_{y2} = 0.16$ m).

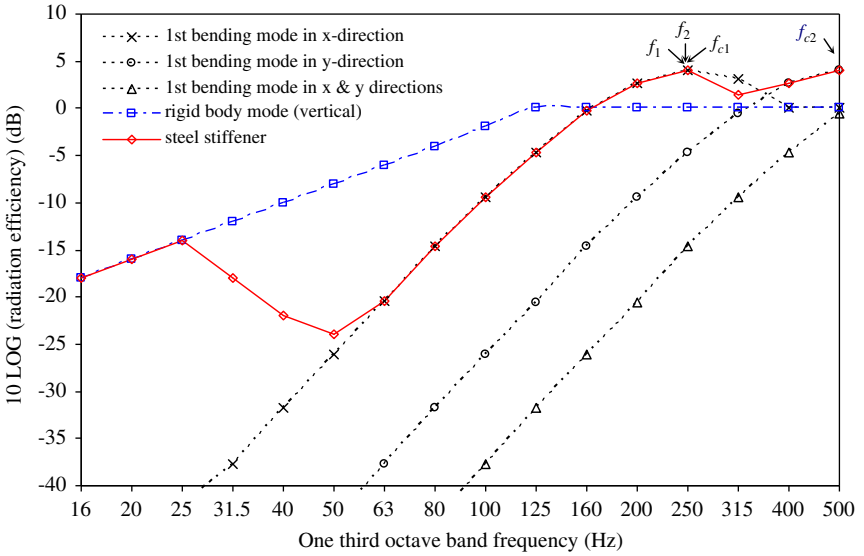

Fig. 13. Theoretical radiation efficiency of wooden panel with steel stiffener (stiffener located at $h_{y2} = 0.16$ m).

The sound pressure levels radiating from the panels with isolator at nodal points are shown in Fig. 16. There is an improvement in sound reduction of the wooden stiffened panel, except for slightly higher sound pressure levels at 100 and 125 Hz bands of the bending resonance. Thus, combining the nodal line stiffener, nodal point isolator and low radiation efficiency at bending resonance can achieve higher noise and vibration isolation improvement.

4. Field measurement

4.1. Specimen installation

Field tests were performed to verify the theoretical results. The equipment setup is illustrated in Fig. 14a. The dimensions and material properties of the tested ceiling panel are given in Table 2. Vibration tests were performed on a single wooden ceiling panel with and without stiffener, and the isolators were located at the edge and nodal positions, respectively.

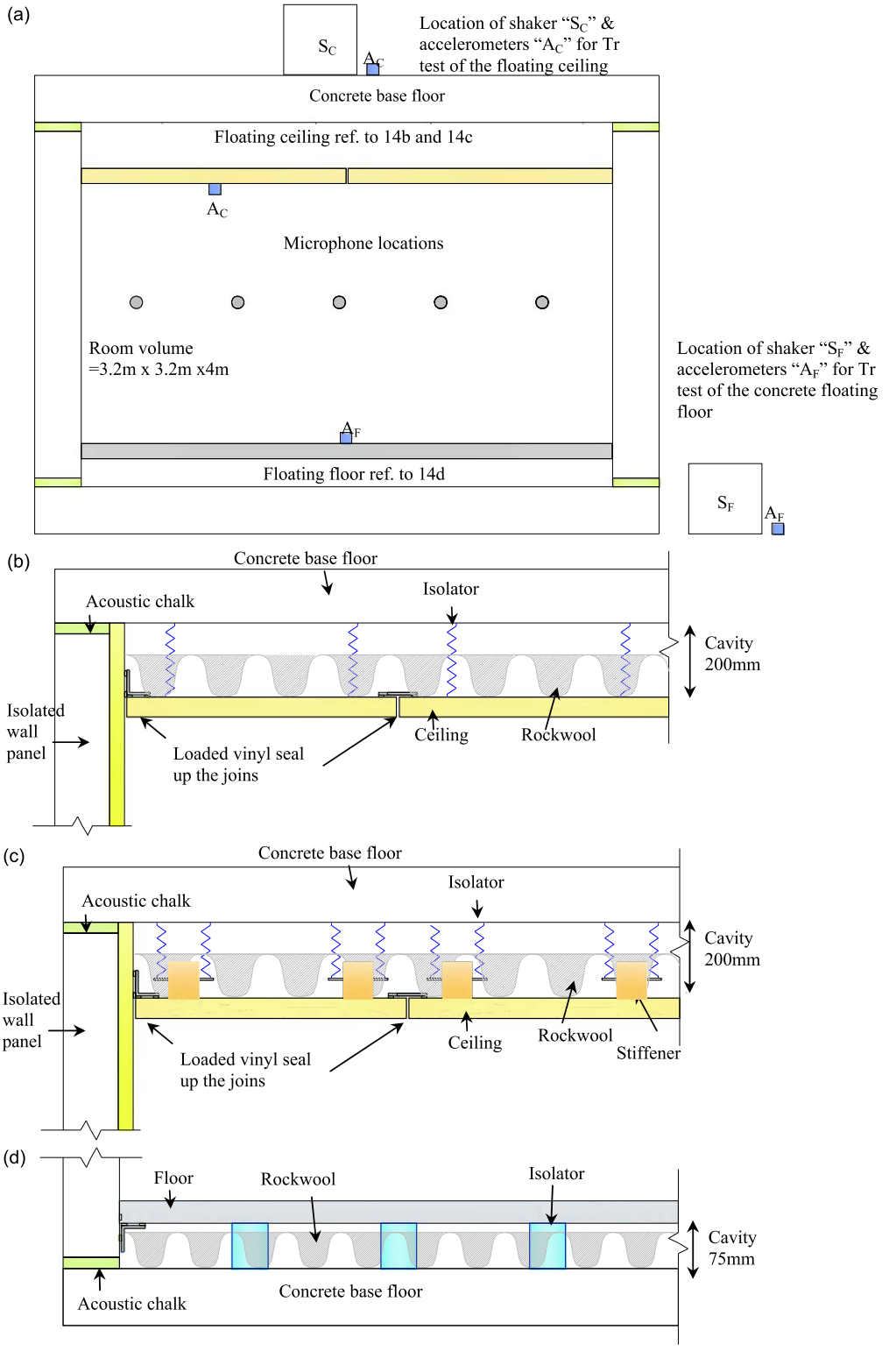

Fig. 14. (a) Experimental set-up in the studio. (b) Construction of floating ceiling with no stiffener. (c) Construction of floating ceiling with stiffener. (d) Construction of floating floor (not to scale).

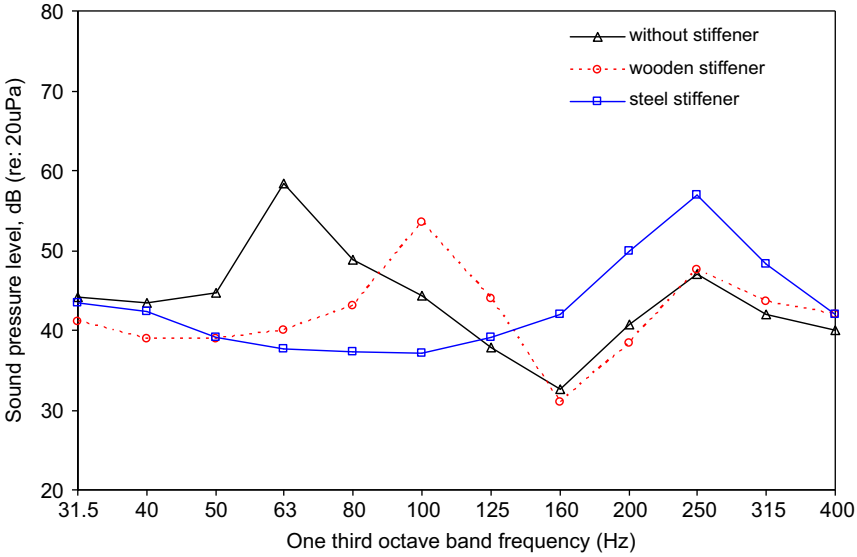

Fig. 15. Theoretical structural radiated sound from wooden panel, and stiffened wooden panel, with isolators placed at four corners (all stiffener located at $h_{y2} = 0.16$ m).

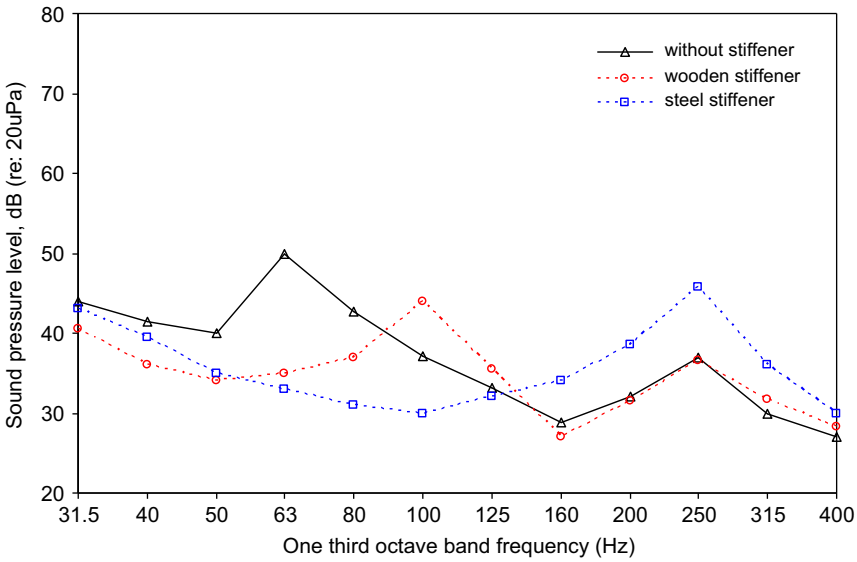

Fig. 16. Theoretical structural radiated sound from wooden panel, and stiffened wooden panels, with isolators placed at four nodal points (all stiffener located at $h_{y2} = 0.16$ m).

Table 3
Bending resonance frequencies (f_1, f_2) and modal critical frequencies (f_{c1}, f_{c2}) of floating panel design (one-third octave band frequency).

Material	1st symmetric mode in x-direction (Hz)		1st symmetric mode in y-direction (Hz)	
	f_1	f_{c1}	f_2	f_{c2}
Plain wooden panel	63	250	250	500
Wooden stiffened panel	100	250	250	500
Steel stiffened panel	250	250	250	500

The plain wooden ceiling was suspended on the roof using the Kinetics Model SH series spring isolators. The total dynamic stiffness of the four isolators was $3.27 \times 10^5\,\mathrm{N\,m^{-1}}$ to achieve the 12 Hz vertical isolator resonance (Fig. 14b). For the ceiling panel with two parallel stiffeners along x-direction, a screw was drilled through the stiffener for suspending the Kinetics Model SH series spring isolators as described in Fig. 14c. The total dynamic stiffness of the eight isolators for each panel was $3.82 \times 10^5\,\mathrm{N\,m^{-1}}$ to achieve the 12 Hz vertical isolator resonance. The typical cavity depth between the floating panels and base was 0.2 m. The acoustic path was insulated using rockwool.

In the acoustic test, eight pieces of identical ceiling panels were installed on the whole ceiling to identify the final sound performance in the studio room. All the joints between floating ceiling and wall, and between two panels were sealed up with a loaded vinyl sheet, which is a flexible and highly damped material.

The floor of the studio was constructed with concrete floating floor (density $= 2400\,\mathrm{kg\,m^{-3}}$) 0.07 m thick; the total stiffness of the 25 pieces of 0.075 m thick Kinetics KIP fibreglass pads was $4.24 \times 10^7\,\mathrm{N\,m^{-1}}$ to obtain the vertical natural frequency of 25 Hz. The cavity depth between the floating floor and base was 0.075 m. The acoustic path was insulated using rockwool. All the joints of the floating floor and wall were also sealed up with the loaded vinyl sheet.

4.2. Vibration measurements

A wooden panel without stiffener and another with wooden stiffener were installed on the nodal lines in x-direction and the vibration transmissibility tests were performed.

A sinusoidal signal was used to drive the 120-N shaker at discrete frequencies (30–400 Hz), a force that rested on the base floor above the tested ceiling, and an accelerometer was mounted on the base to register the input acceleration to the panels. Another accelerometer was mounted at various points on the panels to measure their acceleration response. The two acceleration signals were fed into the analyzer and a computer for data processing. The frequency response function (FRF; the acceleration on the panel/base) was the motion transmissibility and was obtained for the frequency span of 400 Hz (1 Hz resolution). Furthermore, the test of motion transmissibility was also performed on the concrete floating floor, with the shaker being moved to the floor next to the floating floor (Fig. 14a).

4.3. Vibration results

Field measurement results show that the vibration mode shapes and nodal points for two of the floating ceiling designs are the same, although the resonance frequencies are different. The identified mode shapes of fundamental bending resonances in x- and y-directions of one of the panels (panel without stiffener) are sketched in Fig. 17b. The common nodal points of first symmetric bending mode in x- and y-directions shown in Fig. 17c agree very well with theoretical analysis (Fig. 7). However, it is noted that in the graph of first symmetric mode along x-direction there is a small amount of bending along the y-direction instead of rigid body motion, as predicted in Fig. 3. This should decrease the low frequency sound radiation.

The motion transmissibility at centre point of two floating panels with and without stiffener with the isolators located at the corners is shown in Fig. 18. The resonance frequency of the panel without stiffener is at 64 and 250 Hz; the wooden stiffened panel is at 103 and 252 Hz. Compared with the stiffened panel, the fundamental bending resonance frequency increased from 64 to 103 Hz for the wooden stiffener, and the amplification of vibration at 64 Hz was reduced.

When the isolators are placed at nodal points (Fig. 19), the motion transmissibility at resonances can be reduced significantly; +5 dB reduced to −8 dB at 64 Hz for the panel without stiffener, and −4 dB reduced to −18 dB at 103 Hz for the wooden stiffened panel. The vibration of the panel with wooden stiffener becomes less than that without stiffener at the frequency below 90 Hz. The general trend agrees with the theoretical predictions in Figs. 6 and 8.

The comparison of motion transmissibility at the centre point of the wooden stiffened panel and the 0.07 m thick concrete floating floor are presented in Fig. 20. The wooden floating ceiling can achieve a larger vibration reduction than that of the concrete floating floor below 90 Hz, although it has only $\frac{1}{3}$ of the weight of the floor. The stiffness due to the air cavity has no measurable effect on the isolator resonances for the stiffened floating ceiling panel at around 12 Hz, since there is air leakage; this air leakage between panels and the wall will probably be associated to noise leakage in the mid-high frequency range. However, the stiffness in the air cavity may cause the higher vertical natural frequency on the floating concrete floor near 30 Hz, which is close to the first bending resonance of 35 Hz.

A floating ceiling can obtain a lower isolator resonance of 12 Hz, since a spring isolator can be employed in the larger space available and thus lower static loading. There are some practical limitations on the construction of a floating floor; for instance, to limit the additional static deflection due to weight of equipment and furniture, etc. on the floor, a spring isolator may not be applicable. Comparatively, a floating floor cannot be constructed with smaller separated panels like the floating ceiling because of the effect of human activities, and thus the floating floor will have a lower bending resonance frequency than that of the floating ceiling.

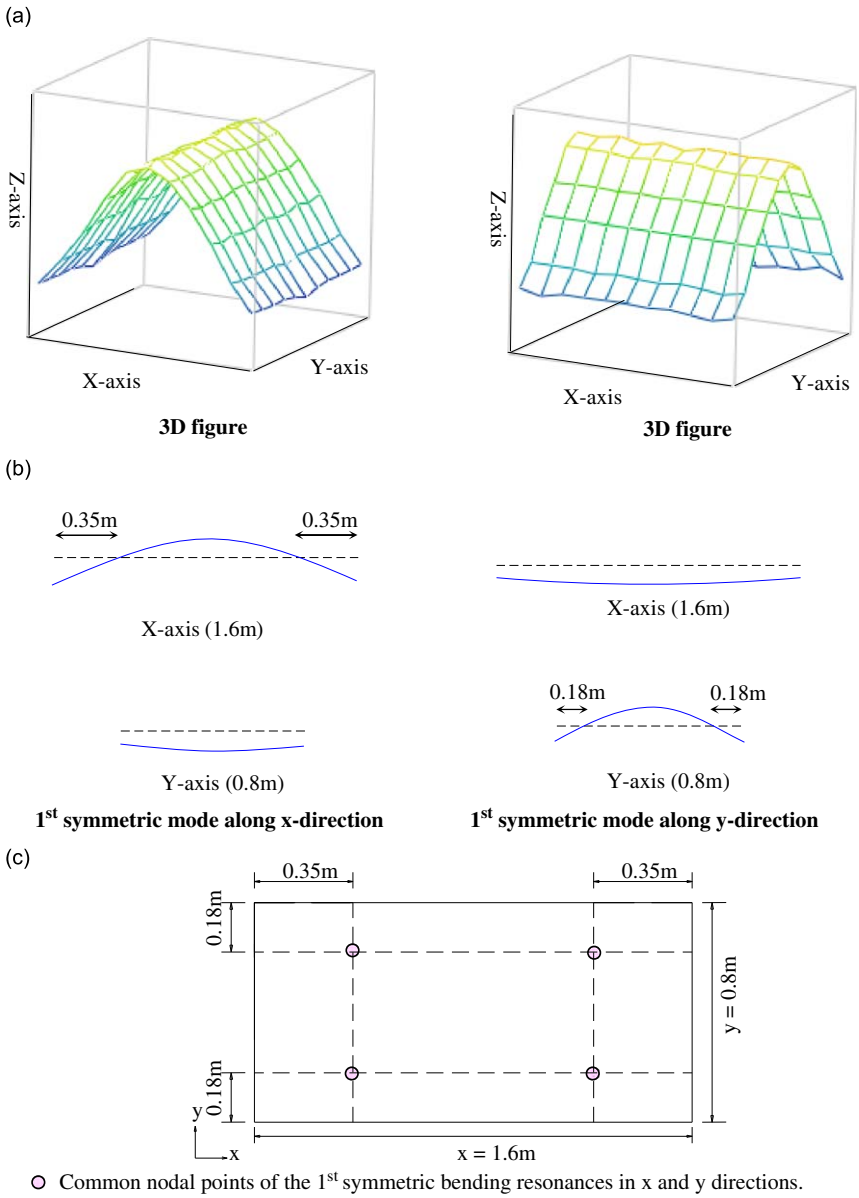

Fig. 17. (a) Mode shape in 3-D figure. (b) Side view of mode shape. (c) Identified nodal points for the lowest two symmetric bending modes.

4.4. Structural radiated noise measurements

On the basis of the above analysis, the optimum design should be the panel with wooden stiffener installed along nodal lines in *x*-direction and the isolator placed at nodal points. Eight pieces of identically designed panels were constructed and installed to cover the whole ceiling of the studio.

The test of structural radiated noise measurements was conducted, and sound pressure levels radiating from floating panels were measured inside a studio room. The average sound pressure levels of all five microphones (Fig. 14a) were presented in one-third octave bands from 31.5 to 400 Hz.

4.5. Structural radiated noise results

The comparison of structural radiated sound from lightweight wooden stiffened panel and concrete floating floor are presented in Fig. 21. The general trends of radiated sound from the floating ceiling are similar to the prediction in Fig. 16.

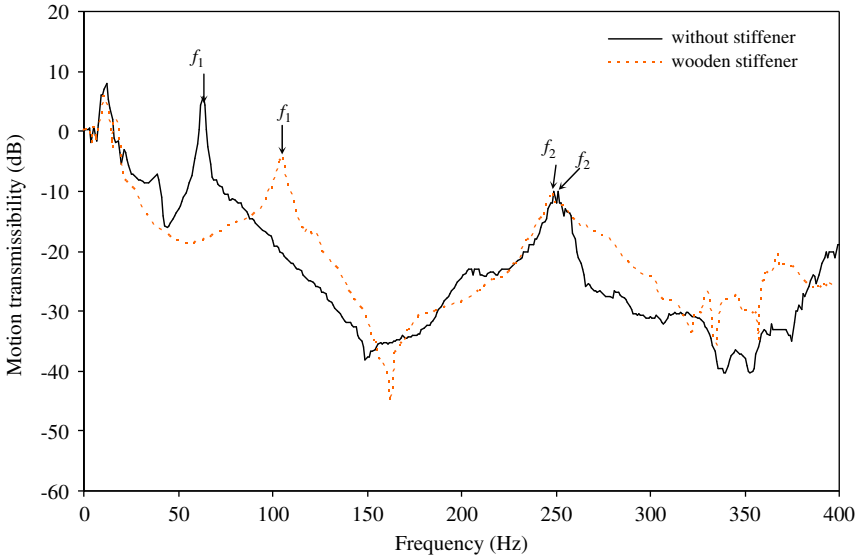

Fig. 18. Measured motion transmissibility of wooden panel, and stiffened wooden panel, with isolators placed at four corners (all stiffener located at $h_{y2} = 0.16$ m).

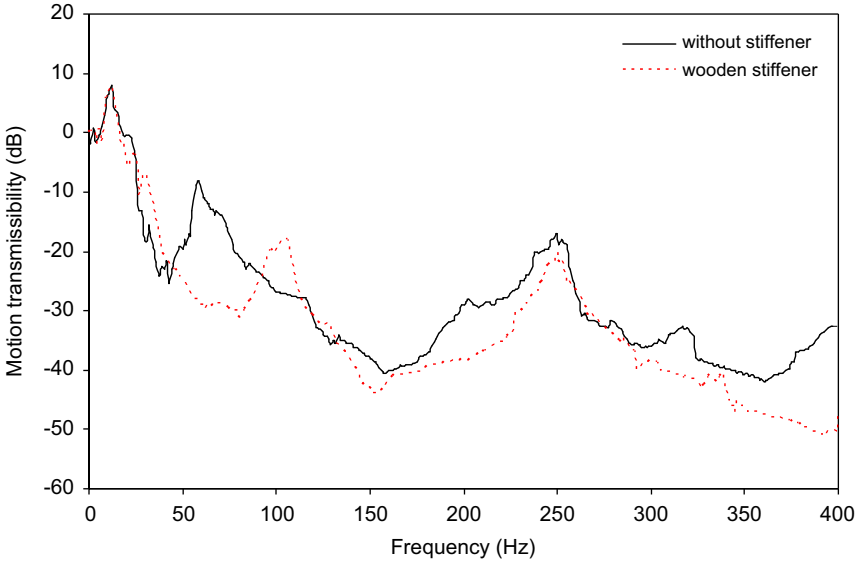

Fig. 19. Measured motion transmissibility of wooden panel, and stiffened wooden panel, with isolators placed at four nodal points (all stiffener located at $h_{y2} = 0.16$ m).

The peaks at 100 and 250 Hz bands correspond to the bending vibration resonances. The radiated sound pressure levels in low frequency below 80 Hz band are higher for the concrete floor due to the higher vibration transmission (Fig. 20).

The test confirmed results in Fig. 1, which state that radiated sound improvement in the frequency range below 125 Hz due to floating ceiling can be higher than that of floating floor, although the weight of the ceiling is usually much lower than that of the floor. To reduce noise at frequencies above 200 Hz, a double ceiling panel similar to the typical double-glazed window may be applied.

5. Conclusion

After extensive analyses conducted to examine the effects of vibration transmission and radiated noise of floating panels with different stiffener design cases in the frequency range of 30–400 Hz, there are four significant findings: (1) Stiffener beams installed at nodal lines along x-direction can increase the first bending resonances in x-direction effectively, and

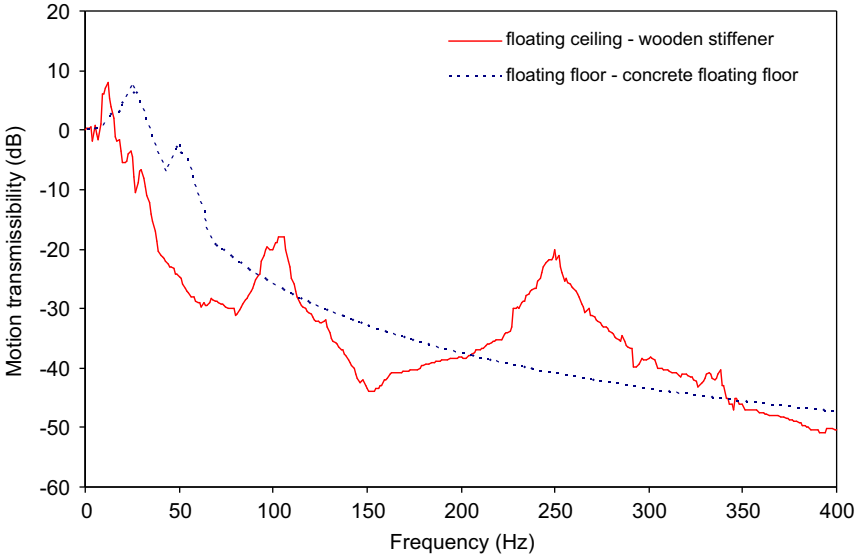

Fig. 20. Comparisons of the measured motion transmissibility of stiffened wooden ceiling and concrete floating floor.

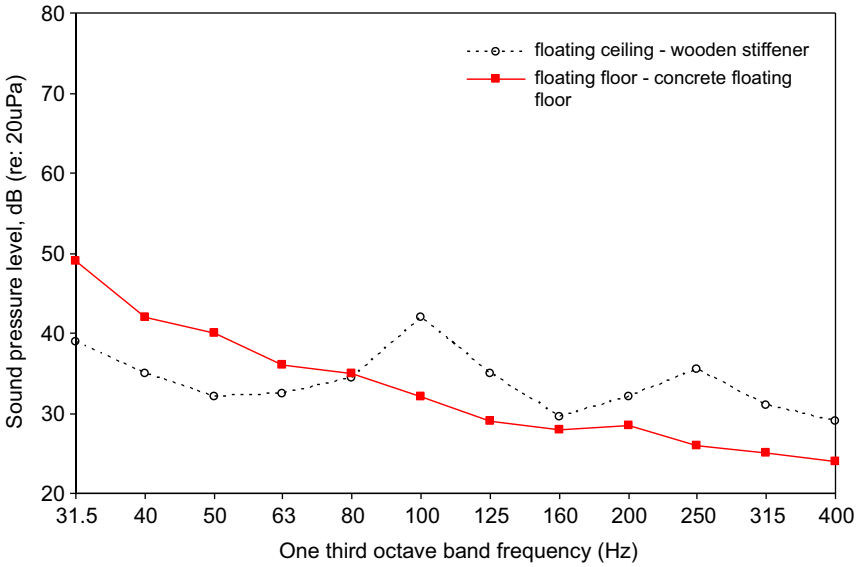

Fig. 21. Comparisons of the measured radiated sound of stiffened wooden ceiling and concrete floating floor.

thus the vibration transmission can be decreased significantly. (2) Modal critical frequency is determined by the size of panel and the corresponding resonance mode shape. The radiation efficiency becomes very large when the first bending resonance frequency is near the modal critical frequency of the fundamental mode. (3) The first bending mode of free–free plate has lower radiation efficiency than that of the simply supported plate; therefore the joints between the panels should be free. (4) Compared with results of the non-stiffened panel, the noise radiated from the stiffened panel can be decreased at non-resonance frequency, but increased at resonance region. However, the peak noise at resonance region is much lower than that of the non-stiffened panel.

In general, to achieve the optimum noise reduction performance, the following design features should be considered: (1) Size of panel—the smaller the panel, the higher the bending resonance frequency and modal critical frequency of the first resonance mode. However, there may be more joints between the panels and careful installation is required. (2) Location of stiffener beam and isolator—stiffener beams should be installed at nodal lines along x-direction, and the isolators can be located at the four nodal points of the first three resonance modes. When the stiffener beams are located at the nodal lines, isolators can be easily installed on the stiffeners. (3) Wavelength mismatch—the fundamental bending

resonance frequency must not match the critical modal frequency so as to prevent the bending resonance from becoming a strong noise radiator.

The new floating ceiling design achieved a vibration reduction of 20 dB in the low frequency range of 40–100 Hz. There is an improvement in sound insulation especially in the low frequency range below 100 Hz band, compared with the conventional design method. The new stiffener and isolators design method should be applicable for a large floating ceiling as well as floating floor.

Acknowledgement

The work that is described in this paper was fully supported by the Hong Kong Polytechnic University Research Fund for Niche Area for Sound and Vibration Research.

Appendix A. Radiated sound power of free–free plate

List of symbols for Appendix

a	length of panel, along x-axis (m)
b	length of panel, along y-axis (m)
c	speed of sound ($\mathrm{m\,s^{-1}}$)
C	room constant ($\mathrm{m^2}$)
DI	directivity factor
I_m, I_n	dummy variable which is a function of m and is equal to the integral over ξ and η in the Rayleigh integral, respectively
i	imaginary number $\sqrt{-1}$
l	radial distance from a point in the far field to the center of the plate (m)
p_r	radiated pressure, Pa
Q	amplitude of displacement (m)
Q_{mn}	modal displacement (m)
q	transverse plate displacement (m)
S_u	surface area of uth surface ($\mathrm{m^2}$)
t	time (s)
$\langle \bar{V}^2 \rangle$	quadratic velocity of the vibrating structure average over the surface $(\mathrm{m\,s^{-1}})^2$
W	sound power (W)
x, y, z	Cartesian coordinates for a point in the far field (m)
$\overline{\alpha}$	average room absorption coefficient
α_u	absorption coefficient of uth surface
θ	polar angle location of a point in the far field (rad)
ξ, η	coordinates for a point on the plate (m)
ρ	mass density of air ($\mathrm{kg\,m^{-3}}$)
σ	radiation efficiency
ϕ	azimuthal angle location of a point in the far field (rad)
ω	angular frequency of excitation ($=2\pi f$) ($\mathrm{rad\,s^{-1}}$)
$Sag(\,)$	sign (either 1 or -1) of the variable in parentheses
m, n	Subscript—m and n is associated with mode shapes functions as defined in Eq. (A.2))

The forcing pressure is harmonic, the steady-state plate displacement will be harmonic such that

$$q(\xi,\eta,t) = Q(\xi,\eta)\,\exp(\mathrm{i}\omega t) \tag{A.1}$$

The free boundary conditions gives

$$Q(\xi,\eta) = \sum_{m=1}^{\infty}\sum_{n=1}^{\infty} Q_{mn}\,\cos\left(\frac{m\pi\xi}{a}\right)\cos\left(\frac{n\pi\eta}{b}\right) \tag{A.2}$$

The plate vibrations cause radiated pressure. The equation relating plate velocity to the radiated pressure can be derived from Green's function formula [16] starting from the basic fluid flow conservation equations together with the Kirchoff–Helmhotz method of integration.

The resulting equation for radiated pressure is commonly known as the Rayleigh integral and is given by

$$p_r(l,\theta,\phi) = \int_{\xi'=-a/2}^{a/2}\int_{\eta'=-b/2}^{b/2} \frac{\mathrm{i}\rho\omega}{2\pi l'}\frac{\partial q(\xi',\eta',t)}{\partial t}\exp(-\mathrm{i}\omega l'/c)\,\mathrm{d}\xi'\,\mathrm{d}\eta'$$

$$\xi' = \xi - \frac{a}{2};\quad \eta' = \eta - \frac{b}{2};\quad l' = \sqrt{(x-\xi')^2 + (y-\eta')^2 + z^2} \tag{A.3}$$

The transmission geometry is given in Fig. 9. Since

$$l = \sqrt{x^2+y^2+z^2};\quad x = l\,\sin\theta\,\cos\phi \quad \text{and} \quad y = l\,\sin\theta\,\sin\phi$$

the equation for l' can be rewritten as

$$l' = l\sqrt{1 - \frac{2\sin\theta\cos\phi}{l}\xi' + \left(\frac{\xi'}{l}\right)^2 - \frac{2\sin\theta\sin\phi}{l}\eta' + \left(\frac{\eta'}{l}\right)^2} \tag{A.4}$$

The integral in Eq. (A.3) must be evaluated numerically. However, a closed-form solution for this integral can be obtained in the far field. In the far field, the following approximations are valid [17]:

$$\frac{1}{l'} \approx \frac{1}{l} \quad \text{and} \quad \exp(-\mathrm{i}\omega l'/c) \approx \exp\left[-\mathrm{i}(\omega/c)l\left(1 - \frac{\sin\theta\cos\phi}{l}\xi' - \frac{\sin\theta\sin\phi\eta'}{l}\right)\right]$$

Thus, the far-field radiated pressure is given by

$$p_r(l,\theta,\phi) = \frac{\mathrm{i}\rho\omega}{2\pi l}\int_{-a/2}^{a/2}\int_{-b/2}^{b/2}\frac{\partial q(\xi',\eta',t)}{\partial t}\exp\left[-\mathrm{i}kl\left(1 - \frac{\sin\theta\cos\phi}{l}\xi' - \frac{\sin\theta\sin\phi}{l}\eta'\right)\right]\mathrm{d}\eta'\,\mathrm{d}\xi' \tag{A.5}$$

Plate motion is assumed to be continuous through the thickness of the plate so that $q(\xi,\eta,t)$ is given by Eqs. (A.1) and (A.2). Thus,

$$\frac{\partial q(\xi,\eta,t)}{\partial t} = \mathrm{i}\omega\left[\sum_{m=1}^{\infty}\sum_{n=1}^{\infty}Q_{mn}\cos\left(\frac{m\pi\xi}{a}\right)\cos\left(\frac{n\pi\eta}{b}\right)\right]\exp(\mathrm{i}\omega t) \tag{A.6}$$

Substituting Eqs. (A.6) into (A.5) allows a closed-form solution to be obtained for the Rayleigh integral as follows:

$$p_r(l,\theta,\phi) = \frac{-\omega^2\rho ab}{2\pi l}\exp\left\{\mathrm{i}\omega\left[t - \frac{l}{c} - \frac{\sin\theta}{2c}(a\cos\phi + b\sin\phi)\right]\right\}\sum_{m=1}^{\infty}\sum_{n=1}^{\infty}Q_{mn}I_mI_n \tag{A.7}$$

where

$$I_m = \begin{cases} -\dfrac{\mathrm{i}}{2}\mathrm{sgn}(\sin\theta\cos\phi) & ((m\pi)^2 = [\sin\theta\cos\phi(\omega a/c)]^2) \\ \dfrac{m\pi\{1-(-1)^m\exp[\mathrm{i}\sin\theta\cos\phi(\omega a/c)]\}}{(m\pi)^2 - [\sin\theta\cos\phi(\omega a/c)]^2} & ((m\pi)^2 \neq [\sin\theta\cos\phi(\omega a/c)]^2) \end{cases}$$

$$I_n = \begin{cases} -\dfrac{\mathrm{i}}{2}\mathrm{sgn}(\sin\theta\sin\phi) & ((n\pi)^2 = [\sin\theta\sin\phi(\omega b/c)]^2) \\ \dfrac{n\pi\{1-(-1)^n\exp[\mathrm{i}\sin\theta\sin\phi(\omega b/c)]\}}{(n\pi)^2 - [\sin\theta\sin\phi(\omega b/c)]^2} & ((n\pi)^2 \neq [\sin\theta\sin\phi(\omega b/c)]^2) \end{cases}$$

The radiated sound power and radiation efficiency are given by

$$\sigma = \frac{W}{\rho c\langle\overline{V}^2\rangle ab} \tag{A.8}$$

where

$$W = \int_{\phi=0}^{2\pi}\int_{\theta=0}^{\pi/2}\frac{p_r^2(l,\theta,\phi)}{2\rho c}l^2\sin\theta\,\mathrm{d}\theta\,\mathrm{d}\phi$$

$$\langle\overline{V}^2\rangle = \frac{1}{4ab}\sum_{1}^{\infty}\sum_{1}^{\infty}Q_{mn}^2$$

To predict the sound pressure level (dB) inside a room Eq. (A.9) should be applied:

$$SPL = SWL + 10\log\left(\frac{DI}{4\pi l^2} + \frac{4}{C}\right) \tag{A.9}$$

where

$$C = \frac{\sum S_u\alpha_u}{1-\overline{\alpha}}$$

References

[1] P. Sipari, *Studies on Impact Sound Insulation of Floor*, VTT Building and Transport, Finland, 2002.
[2] W.E. Blazier, R.B. Dupree, Investigation of low-frequency footfall noise in wood-frame, *multifamily building construction, Journal of the Acoustical Society of America* 69 (3) (1994) 1521–1532.
[3] S. Hveem, Comparison of low frequency impact sound insulation of different Nordic lightweight floor constructions, *Proceedings of Acoustic Performance of Medium-rise Timber Buildings*, Dublin, Ireland, December 1998.

[4] P. Sipari, Sound insulation of multi-storey houses, a summary of Finnish impact sound results, *Building Acoustic* 7 (1) (1999) 15–30.
[5] M. Wollström, Floating floors, models and simulations of vibration characteristics, Report 2000:31, Railway Technology, Department of Vehicle Engineering, Royal Institute of Technology (KTH), Sweden, 2000.
[6] K.W. Ngai, C.F. Ng, Structure-borne noise and vibration of concrete box structure and rail viaduct, *Journal of Sound and Vibration* 255 (2) (2002) 281–297.
[7] J.Y. Jeon, S.Y. Yoo, Effects of the structural stiffness of concrete slabs on floor impact sounds, *Proceedings of Inter-noise*, 2006.
[8] M. Mirowska, Effect of low-frequency noise at low levels on human health in light of questionnaire investigation, *Internoise Special*, 2000, pp. 41–45.
[9] S. Marburg, H.J. Beer, J. Gier, H.J. Hardtke, R. Rennert, F. Perret, Experimental verification of structural-acoustic modeling and design optimization, *Journal of Sound and Vibration* 252 (4) (2002) 591–615.
[10] A. Berry, J. Nicolas, Structural acoustics and vibration behavior of complex panels, *Applied Acoustics* 43 (3) (1994) 185–215.
[11] C.K. Hui, C.F. Ng, New floating floor design with optimum isolator location, *Journal of Sound and Vibration* 303 (1–2) (2007) 221–238.
[12] L.L. Beranek, *Noise and Vibration Control*, rev ed., Institute of Noise Control Engineering, Washington, DC, 1988.
[13] Yi. Yun, C.M. Mak, S.K. Tang, A study of the effect of inertia blocks on the stability of the vibratory system and the performance of vibration isolation, *Applied Acoustics* 68 (2007) 1511–1524.
[14] A. Berry, J.L. Guyader, J. Nicolas, A general formulation for the sound radiation from rectangular, baffled plates with arbitrary boundary conditions, *Journal of the Acoustical Society of America* 88 (6) (1990) 2792–2802.
[15] R.D. Blevins, *Formula for Natural Frequency and Mode Shape*, Yan Nostrand Reinhold Company, New York, 1979.
[16] L.E. Kinsler, A.R. Frey, *Fundamentals of Acoustics*, fourth ed., Wiley, New York, 2000.
[17] F. Fahy, *Sound and Structural Vibration: Radiation, Transmission, and Response*, Academic Press, London, Orlando, 1985.
[18] A.D. Pierce, *Acoustics: An Introduction to its Physical Principles and Applications*, McGraw-Hill, Inc., New York, 1989.
[19] J. Park, L. Mongeau, T. Siegmund, Influence of support properties on the sound radiated from the vibrations of rectangular plates, *Journal of Sound and Vibration* 264 (2003) 775–794.
[20] F.T.K. Au, M.F. Wang, Sound radiation from forced vibration of rectangular orthotropic plates under moving loads, *Journal of Sound and Vibration* 281 (3–5) (2005) 1057–1075.